van der Waals binding energies and intermolecular vibrations of carbazole·R (R=Ne, Ar, Kr, Xe)

Thierry Droz, Thomas Bürgi, and Samuel Leutwyler
Institut für Anorganische, Analytische und Physikalische Chemie, Freiestr.3, 3000 Bern 9, Switzerland

(Received 6 March 1995; accepted 8 June 1995)

Mass-selective ground-state vibrational spectra of jet-cooled carbazole·R (R=Ne, Ar, Kr, and Xe) van der Waals complexes were obtained by populating ground-state intra- and intermolecular levels via stimulated emission pumping, followed by time delayed resonant two-photon ionization of the vibrationally hot complex. By tuning the dump laser frequency, S_0 state vibrational modes were accessed from $\approx$200 cm^{-1} up to the dissociation energy D_0. Upon dumping to ground-state levels above D_0, efficient vibrational predissociation of the complexes occurred, allowing us to determine the S_0 state van der Waals binding energies very accurately. The $D_0(S_0)$ values are $<214.5\pm0.5$ cm^{-1} (R=Ne), 530.4 ± 1.5 cm^{-1} (R=Ar), 687.9 ± 4.0 cm^{-1} (R=Kr), and 890.8 ± 1.6 cm^{-1} (R=Xe). In the S_1 state, the corresponding binding energies are larger by 9% to 12%, being $<222.9\pm1.0$ cm^{-1}, 576.3 ± 1.6 cm^{-1}, 756.4 ± 4.5 cm^{-1}, and 995.8 ± 2.5 cm^{-1}, respectively. © *1995 American Institute of Physics.*

I. INTRODUCTION

Weakly bound van der Waals (vdW) complexes between aromatic molecules (M) and rare-gas atoms (R) have become prototype systems for the investigation of solvation at a microscopic level, especially with respect to spectroscopic properties,[1–3] intermolecular vibrational redistribution (IVR), and vibrational predissociation (VP).[4–15] Especially for the dynamic studies, the weakness of the vdW bond is an essential feature. Despite extensive research on aromatic vdW complexes, these intermolecular binding energies are still not known to high accuracy. Thus for, e.g., benzene·R complexes, the binding energies have been at the focus of recent experimental and theoretical research.[16–20]

We have recently introduced the *stimulated emission pumping/resonant two-photon ionization* (SEP-R2PI) method for the mass-selective determination of ground-state vdW binding energies and vibronic spectra of jet-cooled aromatic van der Waals complexes and clusters M·R or $M\cdot R_n$, where M is an aromatic molecule (carbazole) and R a solvent atom[21,22] or molecule.[23] The results obtained so far for carbazole·Ar (Refs. 21 and 22) reveal great potential for the investigation of *vibrational states*, *binding energies*, and *dynamics* of weakly bound aromatic vdW systems in the electronic ground state. From the point of view of theory, intermolecular interactions in electronic ground states are much more tractable than excited states, and accurate *ab initio* calculations of molecular properties are now possible.[16–19] Experimentally, the ground-state polarizability and charge distribution of the aromatic molecule are usually characterized much more accurately than for excited states. In the present work, we extend the application of this method to the complexes of carbazole with R=Ne, Kr, and Xe.

SEP-R2PI spectroscopy can be viewed as stimulated emission pumping (SEP) followed by a R2PI detection step, in which hot complexes or clusters are detected mass-specifically. Conventional SEP techniques, in which population losses are monitored (i.e., differential signals are recorded), are well established.[8,9,24–29] In contrast to these techniques, SEP-R2PI spectroscopy probes *only* the ''hot'' M·R S_0-products resulting from the pump/dump process followed by ground-state IVR. The method is essentially background-free, and hence very sensitive, as will be shown below.

Other, conceptually similar pump/probe schemes have been used in studies of complexes of the ground-state vibrational dynamics of vdW complexes.[8,9] Rotational coherence fluorescence depletion is a related technique for the measurement of rotational constants.[30] Ionization-detected stimulated Raman spectroscopy (IDSRS) is also closely related, and has been applied by Felker and co-workers for the detection of intra-[31] and intermolecular[32] vibrational resonances in vdW complexes and clusters. The SEP-R2PI method can also be viewed as a fully resonant Raman variation on the IDSRS method. Pump/probe methods have also been used to determine excited-state IVR rates in aromatic vdW complexes.[33,34]

Limits on vdW binding energies have previously been determined by various methods: excited-state dissociation of M·R complexes has been detected by observation of dispersed fluorescence from the bare M aromatic molecule, following IVR/dissociation of the vdW complex.[4,5,7,10,12,35] In an extension, picosecond time-resolved decay time measurements coupled to dispersed fluorescence emission techniques give information on the state-to-state IVR energy flow as well as on the dissociation energy in the vdW complex.[13,14] Alternatively, the nonobservance of S_1 state vibronic bands in R2PI spectroscopy indicates vibrational predissociation of the vdW complex prior to ionization.[11,36] All these techniques probe the excited state and give only upper limits to the binding energies. Conversely, observation of relaxed fluorescence of the vdW complex following excitation implies that the energy content of the complex is less than the binding energy, and lower limits to vdW binding energies have been so inferred.[7] However in electronically excited states, VP rates usually compete with intramolecular radiative and nonradiative processes [fluorescence, intersystem crossing (ISC), internal conversion (IC)],[13] which may intro-

duce uncertainties in the determination of the binding energy.

Recently Krause *et al.*[37] applied mass-selective threshold pulsed field ionization to obtain information on the photodissociation process of cluster ions. By monitoring both the cluster-ion ($M\cdot R^+$) and product-ion (M^+) channel, *lower* and *upper* limits to the ion-state dissociation energy become accessible. Adding the ionization potential shift (ΔIP) of M·R relative to M results in lower and upper limits for the electronic ground-state binding energy. Therefore, with respect to the measurement of binding energies, this technique is a complementary scheme to the SEP-R2PI method described in this work.

A detailed description of the experimental setup is given in Sec. II. In Sec. III we present and discuss the S_0 and S_1 state binding energies as well as the intermolecular vibrational level structure observed for carbazole·R (R=Ne, Ar, Kr, and Xe), and also correlate and compare the D_0 values of the different vdW complexes. Section IV contains the conclusions.

II. EXPERIMENT

A. Principle of the SEP-R2PI method

A scheme of the method[21,22] is displayed in Fig. 1. Supersonically cooled M·R complexes are pumped at the $S_0 \rightarrow S_1$ 0_0^0 band, shown as step (1) in Fig. 1. A very small fraction—typically $<0.1\%$—of the generated S_1-state complexes absorbs a second photon at the pump laser frequency, and is directly ionized, see Fig. 1. In the dump step, induced by a second tunable laser (2) or (2′), a large fraction—typically 30%–40%—of the excited-state population is transferred back to a specific intra- or intermolecular S_0 vibrational level, at an excitation energy E relative to the vibrationless ground state. The combination of pump (1) and dump (2)/(2′) steps, which are synchronized to within ± 2 ns, define the SEP process. The population transfer efficiency achieved in the SEP process depends on several factors, including laser powers for the pump and dump steps, oscillator strength (f), Franck–Condon factors (FC's), IC as well as ISC rates in the S_1 state and dynamics in the S_0 state. By tuning the dump laser a wide range of ground state vibrational states can be accessed.

Following the SEP process, the vdW complex is left to evolve on the ground-state hypersurface, and can be probed for delay times Δ ranging from 50 ns to 15 μs, see Sec. II B. Initially, rapid relaxation occurs out of the prepared S_0-set of mixed eigenstates; in the limit of high vdW mode densities, rapid dissipative IVR occurs. If $E > D_0(S_0)$, this is followed by vibrational predissociation (VP)—typically on a longer time scale than IVR.[7–9,14] Due to substantial anharmonicities of the intermolecular potential energy surface (PES) and the high vibrational level density, which are both very typical for vdW complexes and clusters,[38,39] vibrational relaxation processes occur already at modest excitation energies of a few 100 cm^{-1}.

The relaxation products are probed in the *probe* step [step (3) in Fig. 1] using single-color R2PI. We distinguish two cases:

(1) If the complex has not dissociated during Δ, i.e., $E < D_0(S_0)$, the product M·R complex can be probed via hot bands or sequence bands. By scanning the dump laser (2) and monitoring the ion signal from the probe laser (3), the ground-state vibrations with energies below the dissociation energy are mapped out; this will be denoted *dump spectrum*. Alternatively, if the dump and pump laser are held fixed, and the frequency of the probe laser is varied, $S_0 \rightarrow S_1$ vibronic spectra of selectively heated complexes are obtained, denoted *probe spectra*. Since the dump laser is tuned to a single vibronic transition, all the complexes are generated with defined total internal vibrational energy by the dump process, i.e., are microcanonically ''hot'' systems. The energy definition disregards the rotational energy spread, which is however low, typically $T_{rot} \approx 2$ K in the beam.

(2) If the M·R species has dissociated (that is $E > D_0$) within the time Δ, the hot ground-state population originating from the SEP process has vanished, hence S_0 vibrations are no longer recorded as *positive* signals in the probe step. Under certain conditions discussed in more detail in Sec. III C it is possible to observe ground-state vibra-

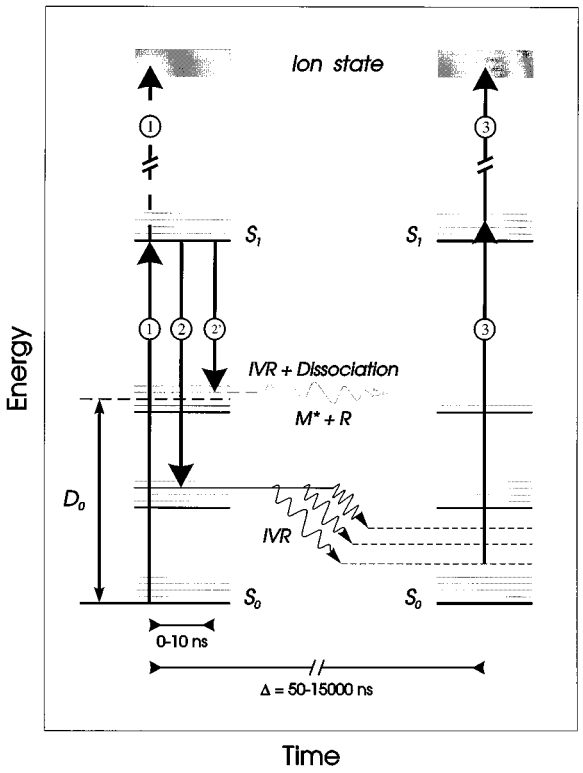

FIG. 1. Schematic level diagram of the stimulated-emission-pumping resonant two-photon ionization (SEP-R2PI) experiment, as applied to a M·R vdW complex. The vertical axis indicates vibrational and/or electronic energy in the M·R complex, the horizontal axis indicates time. In the pump step (1), the M·R complex is excited from S_0 to S_1, usually via the electronic origin. In the dump step (2), vibronic transitions from the S_1 zero-point level are stimulated down to intra- or intermolecular vibrational levels in the S_0 state, which lie below the M·R vdW binding energy (D_0). The system evolves in S_0 during a variable time Δ=50 ns to 15 μs. During this time, IVR leads to population of hot vdW levels. Alternatively, in step (2′), the dump photon populates levels above D_0, leading to vibrational predissociation (VP) during Δ. The population increase (or decrease) in hot vdW levels is then probed by 1+1 resonant two-photon ionization (R2PI) via vdW sequence bands, using photons (3)+(3).

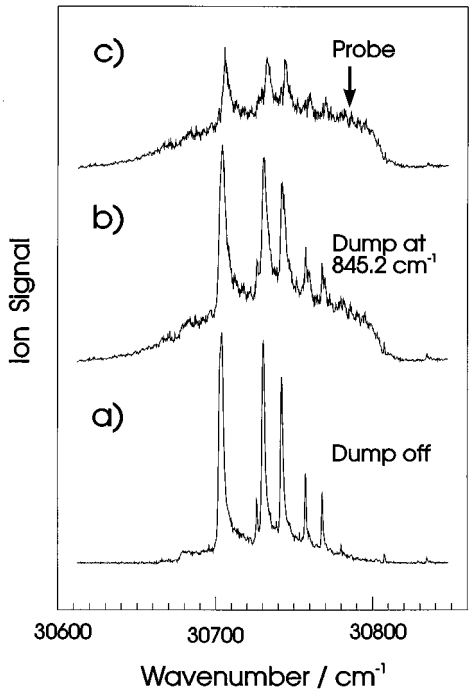

FIG. 2. Probe spectra of the carbazole·Xe complex following the SEP process, using 1+1 resonant two-photon ionization. In trace (a) the pump laser [(1) in Fig. 1] is on, the dump laser (2) is blocked. In (b), both pump and dump lasers are on, dumping occurs to the $\nu_{14}+\nu_3$ intramolecular combination band at 845.2 cm^{-1}, below the vdW bond energy $D_0(S_0)$; note the large increase in broad background in the spectrum. In trace (c), the part of the spectrum due to remaining cold carbazole·Xe population in the beam is subtracted [(c)=(b)−0.7(a)]. Hence, (c) is the spectrum of "hot" S_0 state complexes generated by the pump/dump steps. Note that the residual sharp bands are blue-shifted with respect to spectrum (a).

tions lying above $D_0(S_0)$ as *negative* peaks. Thus, $D_0(S_0)$ is bracketed by the last positively observed and the first negatively or nonobserved S_0 vibrational level.

Figure 2(a) shows a probe laser spectrum of the carbazole·Xe vdW complex in the vicinity of the electronic origin ($S_0 \rightarrow S_1$); for this spectrum the pump laser was on, but the dump laser was off, and $\Delta=750$ ns. In trace (b), the second laser dumps Car·Xe complex population to an S_0 intramolecular combination band at 845.2 cm^{-1}; the probe laser covers the same spectrum as in trace (a). A manifold of hot bands and sequence bands appears as a relatively unstructured background spectrum; superimposed on this is the spectrum of the remaining "cold" Car·Xe complexes which did not undergo the SEP process. In Fig. 2(c), subtraction of the "cold" spectrum (a) from (b) reveals the spectrum of microcanonically hot carbazole·Xe at an internal energy of 845 cm^{-1}. Note that the vibronic bands still present in (c) are wider and less intense than in trace (a), and are *blue-shifted* by nearly 3 cm^{-1}. On the other hand the broad background in the 30 600–30 800 cm^{-1} range without sharp structure reflects the statistical energy redistribution by IVR at a relatively high density of states.

For the dump spectra, the sensitivity depends on the choice of the probe laser frequency. The arrow in Fig. 2(c) marks an optimum position for the probe laser ($\nu_{probe}=30\,790$ cm^{-1}), as the fraction of hot complexes detected at this frequency is relatively large, and the background of cold clusters present without dump laser [Fig. 2(a)] is minimal. The probe-laser frequencies used for the other complexes are given in Sec. III.

The band intensities of the dump spectra depend on (i) the Franck–Condon factors for the $S_1 \rightarrow S_0$ transition; (ii) the S_0 IVR rates from the optically accessed or "bright" state to the background states; (iii) optical saturation: in order to achieve a reasonable downward population transfer, the dump laser intensity was usually high enough to saturate the stronger vibronic transitions, leading to an overestimate of the weaker bands; (iv) the frequency of the probe laser. This effect is most pronounced at low dump frequencies (excess energies), since the mode density is still low and vibrational interstate couplings may be level-dependent. At low excitation energies, the probe spectra are structured, i.e., distinct sequence bands are observed, as was previously shown for Car·Ar (Ref. 21) after dumping to $\nu_3(a_1)$ at 215 cm^{-1}. Since in the dump spectra the probe laser is fixed at a certain frequency, modes for a sequence or hot band that happens to lie at the probe laser frequency are enhanced by the probe step. At higher frequencies, the probe laser spectra are broad and unstructured, but the shape of the probe spectrum can change systematically with excitation energy. For example in Car·Xe, where the probe spectrum is broad and unstructured above 420 cm^{-1} excitation energy, the maximum of the broad spectrum shifts to higher energy when exciting higher vibrational levels.

B. Experimental details

1. Cluster synthesis

Car·R (R=Ne, Ar, Kr, and Xe) clusters were synthesized and cooled in pulsed, seeded supersonic expansions. A magnetically actuated pulsed valve was employed, with a circular nozzle of diameter $D=0.4$ mm and wall thickness 0.2 mm. Gas pulsewidths were 200–250 μs. Carbazole (Fluka AG Switzerland, >99% purity) was heated to 120 °C, giving a vapor pressure of ≈1 mbar, and seeded into either pure neon or mixtures of 2% argon, krypton or xenon in 98% neon carrier gas at a backing pressure $p_0=1.2$ bar. The skimmed molecular beam was probed at a distance $x/D=400$. Details of the molecular beam machine and the linear time-of-flight mass spectrometer system are essentially identical to that of our previous work.[40]

2. Laser system

Three independently tunable nanosecond UV lasers are employed in the experiment. The pump and dump laser pulses [step (1) and (2) or (2′) in Fig. 1] were provided by two frequency doubled dye lasers (FL2002, FL3002, DCM dye), pumped by the same 532 nm output of a Nd:YAG laser (Quanta Ray GCR3). Typical pulse energies were 200 μJ and 1 mJ for pump and dump laser pulses, respectively. Both beams were mutually overlapped in space and time, and crossed the molecular beam perpendicularly within the ion source. The frequency doubled UV output of a third pulse dye laser (FL3002, DCM dye), pumped by a sec-

ond Nd:YAG laser (Quanta Ray GCR 170) was used for the probe. The *Q*-switches of the two Nd:YAG lasers were synchronized with a digital delay generator (Stanford Research DG 535). The crossing point of the probe laser with the molecular beam could be varied from 0 to 13 mm downstream of the pump/dump beams. This is possible due to the relatively large acceptance diameter of the TOF mass spectrometer. With Ne carrier gas, this corresponds to a time delay Δ up to 15 μs. The minimum delay time that could be usefully employed was 50 ns, roughly twice the fluorescence lifetime of the Car·Ar complex.[40] Typical probe laser pulse energy was 300 μJ. All three laser beams were unfocused, and the beam profiles at the molecular beam were approximately 2×2 mm.

3. Fluorescence lifetimes

Carbazole or Car·R complexes R (R=Ne, Ar, Kr, and Xe) were excited at their respective electronic origins, at $x/D \approx 15$. The resulting fluorescence was collected with a quartz lens and detected by a RCA 7265 photomultiplier. The fluorescence decay curves were recorded with a Tektronix DSA-602 2 GHz digitizer and averaged over 1000 laser shots. The data were corrected for the laser pulsewidth and instrument response function via deconvolution. All five decay curves were exponential to within experimental accuracy.

III. RESULTS AND DISCUSSION

A. Carbazole·Kr

1. S_0 ground-state vibrations

We first discuss the intra- and intermolecular vibrational levels of Car·Kr in the frequency range 200–700 cm^{-1}. For all dump spectra the probe frequency was $\nu_{probe}=30\,873$ cm^{-1}, 64 cm^{-1} to the blue of the $S_0 \rightarrow S_1$ origin transition. An overview spectrum is shown in Fig. 3, and two spectrally expanded regions in Fig. 4. The intramolecular modes are classified in the C_{2v} point group symmetry of bare carbazole, although the complex has lower symmetry. The $S_0(A_1) \rightarrow S_1(A_1)$ transition is in-plane and short-axis (y-axis) polarized. The assignment of S_0 intramolecular bands in the Car·Kr SEP-R2PI dump spectrum is based on previous work in molecular beams and low-temperature crystals[41,42] as well as *ab initio* calculations.[22,43] Due to Herzberg–Teller coupling to the $S_2(b_2)$ electronic state, b_2 vibrations also occur with moderate intensities.[41] Note that a_2+b_1 combination bands are also of b_2 symmetry. Beside a_1 and b_2 vibrations, such combination bands are observed in the Car·Kr spectrum at 393.0 cm^{-1} $[\nu_2(a_2)+\nu_4(b_1)]$, 619.4 cm^{-1} $[\nu_5(a_2)+\nu_6(b_1)]$ and 683.9 cm^{-1} $[\nu_2(a_2)+\nu_3(a_1)+\nu_6(b_1)]$. Between 200 cm^{-1} and 700 cm^{-1} the spectrum (Fig. 3) consists of three clumps of bands centered at 240 cm^{-1}, 440 cm^{-1}, and 650 cm^{-1}, respectively. Within the first group, shown in Fig. 4(a), are the strong intramolecular vibrations $2\cdot\nu_1(b_1)$ and $\nu_3(a_1)$. The most prominent bands in the second group are assigned to $\nu_7(a_1)$ and $2\cdot\nu_3(a_1)$, whereas in the third group, presented in Fig. 4(b), $\nu_{14}(b_2)$ and $\nu_{15}(a_1)$ have largest intensity. Table I compiles the observed S_0 vibrational frequencies and intensities.

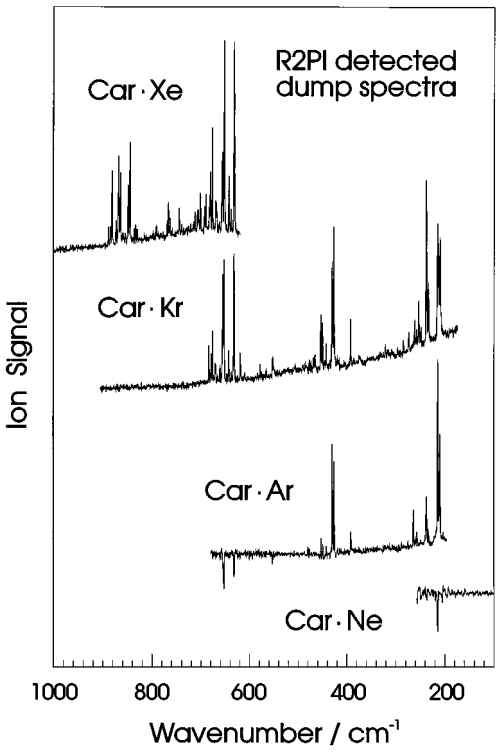

FIG. 3. SEP-R2PI ground-state spectra of carbazole·R (R=Ne, Ar, Kr, and Xe) obtained by tuning the dump laser frequency [step (2), (2′) in Fig. 1]. The scale is given in wave numbers relative to the respective origins 0_0^0, see text.

Many combination bands of intra- with intermolecular vibrations are also observed in the dump spectra. The derived intermolecular vibrational frequencies are also listed in Table I. From these, average values of intermolecular frequencies (averaged over all observed combination bands) are listed in Table II. Vibrational fundamentals of the ν_y and ν_z vdW modes appear in the spectrum, at 23.4 cm^{-1} and 38.8 cm^{-1}, respectively. Assignments are based on earlier work on Car·Ar (Ref. 44) and Car·Kr;[36] ν_y is the in-plane or bending vibration along the short axis of carbazole and ν_z is the out-of-plane or stretching vibration. Both modes are totally symmetric (a') in the complex point group C_s. Earlier determination of these frequencies by dispersed fluorescence emission spectroscopy[36] gave $\nu_y=22.7$ cm^{-1} and $\nu_z=39.0$ cm^{-1}, in good agreement with the present results.

The ν_y mode usually yields the strongest intermolecular combination bands, but the first overtone $2\cdot\nu_y$ as well as the ν_z fundamental are also often observed in combination with strong and moderately strong intramolecular bands. In combination with $\nu_3(a_1)$, which is especially intense, even the second overtone $3\cdot\nu_y$ and the intermolecular combination $\nu_z+\nu_y$ are observed. Here, the inter- plus intramolecular combination band $\nu_3(a_1)+\nu_y$ is even stronger than the intramolecular fundamental $\nu_3(a_1)$ as seen in Figs. 3 and 4(a).

2. Binding energy

The ground-state vdW binding energy $D_0(S_0)$ of Car·Kr was accurately determined by a bracketing measurement. The highest vibrational level which gives a *positive* dump

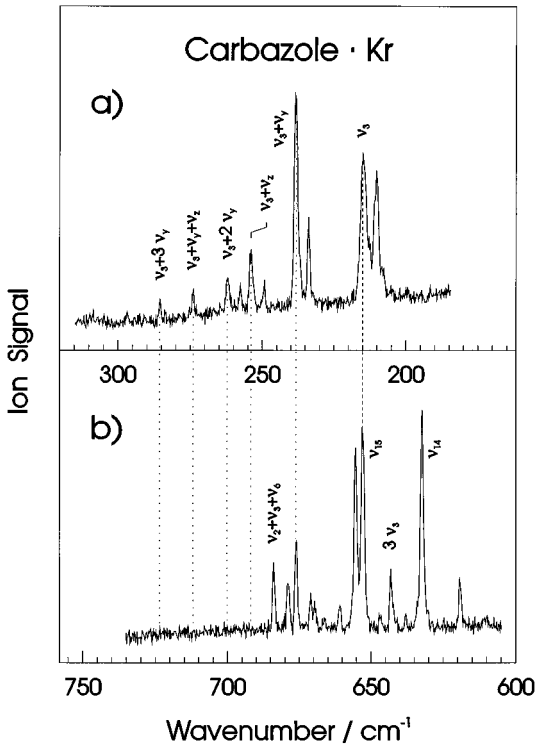

FIG. 4. Expanded regions of the "dump" spectrum of carbazole·Kr (see Fig. 3), showing intermolecular vdW modes (ν_y and ν_z) in combination with the intramolecular levels ν_3 [trace (a)] and ν_{15} [trace (b)], respectively. In order to bring out the missing transitions in trace (b), the two intramolecular transitions ν_3 and ν_{15} are horizontally aligned. The scale is relative to the origin of carbazole·Kr at 30 740.5 cm^{-1}.

spectrum signal lies at 683.9 cm^{-1}, shown in Fig. 4(b). This band corresponds to the $\nu_2(a_2)+\nu_3(a_1)+\nu_6(b_1)$ combination level, observed at 682 cm^{-1} in bare carbazole. This level determines the lower limit of the vdW binding energy. The following vibrational levels expected, but *not observed*, are indicated in Fig. 4; the dotted lines indicate the observed positions of the vdW combination bands of $\nu_3(a_1)$ in Fig. 4(a), and point to the expected positions of the analogous combination bands of $\nu_{15}(a_1)$ in the lower half of Fig. 4(b). One such band is the intra- plus intermolecular combination $\nu_{15}+\nu_z$, expected at 653.1+38.8 cm^{-1}=691.9 cm^{-1}. We note that the $\nu_{15}+\nu_y$ band is strong, but the higher intermolecular combination vibrations, i.e., the ν_z, the $2\cdot\nu_y$, and the $\nu_y+\nu_z$ are clearly missing. Another missing (or very weak) combination band corresponds to the level $\nu_{14}+\nu_y+\nu_z$, expected at 691.3 cm^{-1}. Neither of these, nor any other levels are observed to higher frequency, implying all levels >691.9 cm^{-1} lie above the dissociation limit of the vdW bond. Combination of these two limits bracket the ground-state binding energy of Car·Kr as $D_0(S_0)=687.6\pm3.7$ cm^{-1}.

3. Delay time dependence and dissociation rates

Weber and Rice have performed time-resolved experiments on vdW complexes *s*-tetrazine·R (R=Ar, Kr, Xe) in the electronic ground state, which gave *lower* limits to vibrational redistribution lifetimes of 4–15 ns, depending on the rare gas and the excess energy.[8] This indicates that ground-state IVR/VP processes might be quite slow, for yet unknown reasons. Also, the VP rate decreases as the dissociation limit D_0 is approached from above. For either of these reasons, one might argue that during the delay time Δ=400

TABLE I. Intra- and intermolecular vibrational frequencies and band intensities for ground-state carbazole·Kr, in the 200–700 cm^{-1} range. Intermolecular frequencies are derived from combination bands with intramolecular modes.

Assignment	Wave number/cm^{-1}	Interm./cm^{-1}	Intensity/%[a]
$2\cdot\nu_1$	210.3		61.7
ν_3	215.0		69.3
$2\cdot\nu_1+\nu_y$	233.8	23.5	42.4
$\nu_3+\nu_y$	238.5	23.5	100.0
$2\cdot\nu_1+\nu_z$	249.2	38.9	15.3
$\nu_3+\nu_z$	253.9	38.9	29.3
$2\cdot\nu_1+2\cdot\nu_y^b$	257.6	47.3	12.8
$\nu_3+2\cdot\nu_y^b$	262.0	47.0	16.0
$\nu_3+\nu_y+\nu_z^b$	274.0	59.0	13.5
$\nu_3+3\cdot\nu_y^b$	285.4	70.4	10.2
$\nu_2+\nu_4$	393.0		29.5
ν_7	427.3		91.8
$2\cdot\nu_3$	430.7		63.8
$\nu_2+\nu_4+\nu_z$	443.1		16.2
$\nu_7+\nu_y$	450.5	23.2	34.4
$2\cdot\nu_3+\nu_y$	453.9	23.2	38.7
$\nu_7+\nu_z$	466.1	38.8	10.9
$2\cdot\nu_3+\nu_z$	469.5	38.8	8.5
$\nu_7+2\cdot\nu_y^b$	473.8	46.5	6.8
$2\cdot\nu_3+2\cdot\nu_y^b$	477.5	46.8	8.1
ν_{11}	552.9		13.3
$\nu_{11}+\nu_y$	578.0	25.1	9.2
$\nu_5+\nu_6$	619.4		17.6
ν_{14}	632.3		81.8
$3\cdot\nu_3$	643.2		22.5
ν_{15}	653.1		75.5
$\nu_{14}+\nu_y$	655.4	23.1	67.9
$3\cdot\nu_3+\nu_y$	666.3	23.1	9.1
$\nu_{14}+\nu_z$	671.0	38.7	12.8
$\nu_{15}+\nu_y$	676.0	22.9	33.6
$\nu_{14}+2\cdot\nu_y^b$	678.7	46.4	17.6
$\nu_2+\nu_3+\nu_6$	683.9		25.2

[a]Percentage intensity, relative to strongest band.
[b]Tentative assignment.

TABLE II. Experimental intermolecular vibrational frequencies (in cm^{-1}) for carbazole·R (R=Ar, Kr, and Xe) in the S_0 and S_1 state.[a]

	Vibration	Ar	Kr	Xe
S_0 state	ν_y	22.9	23.4	24.4
	$6\cdot\nu_x^b$	24.4		
	$2\cdot\nu_y^b$	42.3	46.9	49.1
	ν_z	50.0	38.8	37.7
	$\nu_y+\nu_z^b$		59.0	60.4
	$3\cdot\nu_y^b$		70.4	73.3
	$2\cdot\nu_y+\nu_z^b$			83.4
S_1 state	ν_y	23.6	24.5	26.9
	$6\cdot\nu_x^b$	25.9		22.8
	$2\cdot\nu_y^b$	43.6	49.4	54.0
	ν_z	50.8	40.2	38.5
	$\nu_y+\nu_z^b$		61.7	64.6
	$3\cdot\nu_y^b$			77.2

[a]Values refer to band maxima; experimental error ±0.2 cm^{-1}.
[b]Tentative assignment.

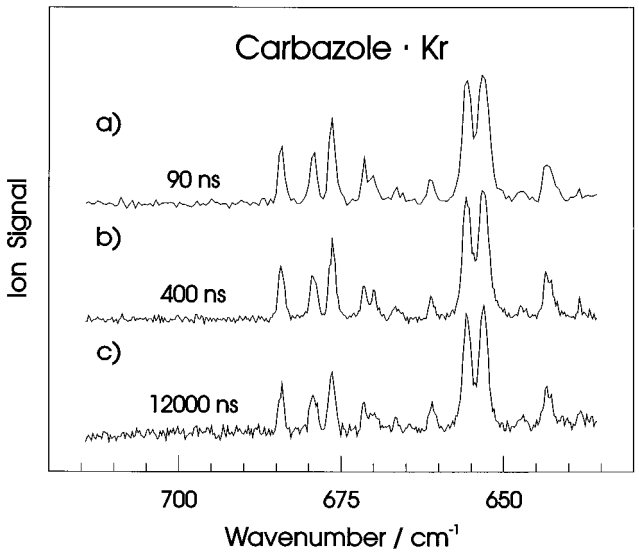

FIG. 5. SEP-R2PI spectra of carbazole·Kr obtained by scanning the dump laser in the vicinity of the ground-state dissociation limit $D_0(S_0)$. The delay times Δ between SEP process and R2PI detection step, are (a) Δ=90 ns, (b) Δ=400 ns, and (c) Δ=12 000 ns. Within experimental accuracy, all traces show identical band positions and relative intensities.

ns employed for the dump spectra in Fig. 4 the vdW complex did not dissociate to an appreciable extent. If S_0-state VP dynamics would indeed extend into this time range, the intensities of bands corresponding to levels lying above D_0 should be delay time dependent. Also, since the VP rate increases with increasing excess energy E^+ ($E^+=E-D_0$), bands corresponding to different levels above D_0 should disappear at different rates with increasing delay time.

In order to investigate this, dump spectra were measured over a spectral range of $\approx$100 cm^{-1} in the vicinity of the dissociation limit, with the probe laser delayed by Δ=90 ns, 400 ns, and 12 μs, covering more than two orders of delay time. As Fig. 5 shows, the spectra show *no* delay time dependence whatsoever between Δ=90 ns to 12 μs, even small details of the relative band intensities being conserved. From this we conclude that (i) even at the lowest excess energy E^+, corresponding to the $\nu_{15}(a_1)+\nu_z$ level, the VP lifetime must be $<$40 ns, given the delay time of 90 ns, the expected signal intensity, and the noise level, corresponding to a lower limit of the VP rate $k_{VP}=2.5\cdot10^7$ s^{-1}. (ii) Since no higher-lying levels are observed, their VP lifetimes must also be $<$40 ns, indicating no detectable variations in VP rates in this energy range. (iii) If the 683.9 cm^{-1} level were above the dissociation energy, as postulated above, its VP lifetime would have to be $>$30 μs, given the Δ=12 μs and the similarity of spectrum in Fig. 5(c) to that in Fig. 5(a). A difference of almost three orders of magnitude in VP rate over a small energy range is highly improbable, and we conclude that the lower experimental limit of $D_0(S_0)$ for Car·Kr is indeed 683.9 cm^{-1}.

The VP rate predicted by the RRKM model is given by

$$k_{VP}(E)=\frac{\Sigma N_v(E^+)}{h\rho(E)},$$

TABLE III. Dissociation energies D_0 (in cm^{-1}) for the S_0 and S_1 state of carbazole·R (R=Ne, Ar, Kr, and Xe).

R	$D_0(S_0)$	$\delta\nu$[a]	$D_0(S_1)$	Increase
Ne	$<$214.5±0.5	−8.5±0.5	$<$222.9±1.0	
Ar	530.4±1.5	−45.9±0.04[b]	576.3±1.6	8.8%
Kr	687.6±3.7	−68.5±0.5	756.1±4.2	10.0%
Xe	890.8±1.6	−105.0±1.0	995.8±2.5	11.8%

[a]Spectral shifts $\delta\nu$ are relative to the carbazole 0_0^0 band at 30 809 cm^{-1}.
[b]Value from Ref. 51.

where E is the total (intra- and intermolecular) vibrational energy, E^+ is the amount of excess vibrational energy above the dissociation threshold D_0 (see definition above), the numerator is the sum of vibrational states exceeding the dissociation energy (but exclusive of the dissociation coordinate), and $\rho(E)$ is the vibrational density of states at energy E. If we employ the lower limit to the VP rate derived above and assume that $\Sigma N_v(E^+)=1$, i.e., E^+ is at the *first* state above the dissociation energy, a vibrational density of states $\rho\approx1200/\text{cm}^{-1}$ is obtained at a total energy corresponding to the vdW dissociation energy. Previous estimates of the vibrational density of states[6,14,15] are one to two orders of magnitude lower than this, indicating that the VP rate predicted by the RRKM model is 10^8–10^9 s^{-1} just above the threshold. This is in agreement with the present observations.

The S_1 *excited-state* binding energy can be determined by adding the spectral red shift of $\delta\nu$=68.5±0.5 cm^{-1} to the ground-state binding energy, giving $D_0(S_1)$=756.1±4.2 cm^{-1}. The measured values for the S_0 ground-state binding energy, the spectral shift $\delta\nu$ and the S_1 excited state binding energy as well as the relative increase of the binding energy upon going from S_0 to S_1 are collected in Table III for Car·R (R=Ne, Ar, Kr, and Xe).

B. Carbazole·Xe

1. S_0 ground-state vibrations

The dump spectrum of Car·Xe in the frequency range 630–890 cm^{-1} is shown in Fig. 3, and expanded in Fig. 6. The probe laser was fixed 71 cm^{-1} to the blue of the 0_0^0 band. Table IV lists the frequencies, intensities, and assignments of the observed transitions. The relative intensities of the intramolecular vibrations in the spectra of Car·Xe and Car·Kr are similar between 630 cm^{-1} and 690 cm^{-1}. Intense bands at 632 cm^{-1} and 653 cm^{-1} are assigned to the ν_{14} and ν_{15} modes, respectively, whereas considerably weaker bands assigned to $3\cdot\nu_3(a_1)$ and $\nu_2(a_2)+\nu_3(a_1)+\nu_6(b_1)$ arise at 643 cm^{-1} and 684 cm^{-1}, respectively. The frequencies of these intramolecular modes agree to within 0.5 cm^{-1} for the Kr and Xe complexes. At energies beyond $D_0(S_0)$ of Car·Kr, further intramolecular modes have been assigned for Car·Xe. The most prominent bands above 840 cm^{-1} are combinations of ν_3 with ν_{14} and ν_{15} at 845.2 cm^{-1} and 868.0 cm^{-1}. Slightly less intense bands arise from $\nu_{21}(b_2)$, $\nu_5(a_2)+\nu_{12}(b_1)$ and $\nu_{22}(a_1)$ modes at 849.1 cm^{-1}, 864.5 cm^{-1} and 881.6 cm^{-1}, respectively.

As for Car·Kr, the two intermolecular fundamentals ν_y and ν_z are active and are observed as combinations with

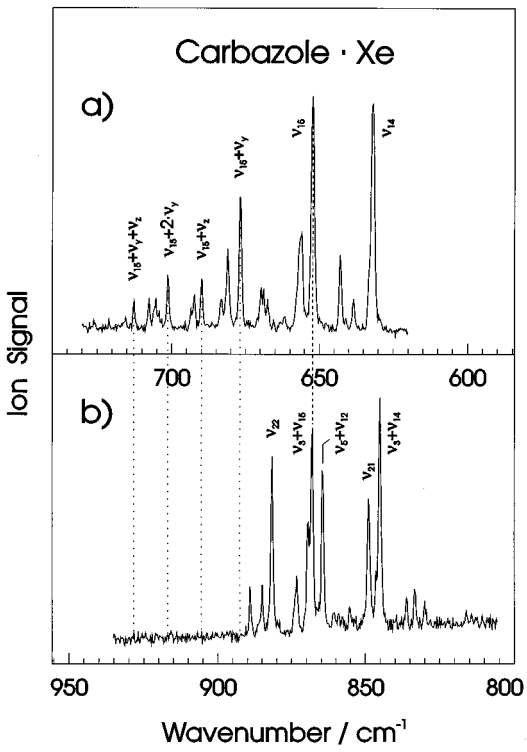

FIG. 6. Expanded regions of the ground-state spectrum of carbazole·Xe, cf. Fig. 3. The spectral regions corresponding to the intramolecular levels ν_{15} [trace (a)] and $\nu_3+\nu_{15}$ [trace (b)], respectively, are shown. In order to point out the bands which are missing in trace (b), the two intramolecular transitions ν_{15} and $\nu_3+\nu_{15}$ are horizontally aligned. The scale is relative to the origin of carbazole·Xe at 30 704.0 cm^{-1}.

intramolecular modes in the dump spectra. Table II compiles intermolecular frequencies as derived from combination bands with intramolecular modes. The average S_0 state fundamental frequencies are 24.4 cm^{-1} and 37.7 cm^{-1} for ν_y and ν_z, respectively. As for Car·Kr, ν_y is observed in combination with all moderately strong bands in the spectrum, the intensity being one third to one half of the corresponding intramolecular band intensity. Beside the very intense ν_y band, ν_z, $2\cdot\nu_y$ and $\nu_y+\nu_z$ are clearly observed in combination with ν_{15}, as shown in Fig. 6(a). Weaker bands are assigned to $2\cdot\nu_y+\nu_z$ and $3\cdot\nu_y$, respectively.

2. Binding energies

An accurate ground-state van der Waals binding energy $D_0(S_0)$ was also obtained for Car·Xe. In Fig. 6(b) the relevant part of the spectrum is expanded; the last observed level, at 889.2 cm^{-1}, corresponds to the intra- plus intermolecular combination level $\nu_5+\nu_{12}+\nu_y$. The next expected level $\nu_3+\nu_{15}+\nu_y$ at 868.0+24.4 cm^{-1}=892.4 cm^{-1} is not observed. Therefore, the bracketing measurement is very accurate, giving a ground-state binding energy of $D_0(S_0)=890.8\pm1.6$ cm^{-1}. In Fig. 6(a), the $\nu_{15}(a_1)$ vibration at 652.4 cm^{-1} serves as an example for the typical pattern of intra- plus intermolecular vibrations. In Fig. 6(b) the dotted lines indicate the corresponding line positions for combinations with the $\nu_3+\nu_{15}$ mode, which are clearly missing. If the dissociation limit were >892.4 cm^{-1}, the $\nu_3+\nu_{15}+\nu_y$ band should have comparable intensity as the last observed band, since both levels correspond to combination bands of an intramolecular vibration with ν_y and the two intramolecular bands are of similar intensity.

Addition of the spectral shift of 105.0 ± 1.0 cm^{-1} yields a dissociation energy in the S_1 first excited state of $D_0(S_1)=995.8\pm2.5$ cm^{-1} (see also Table III).

TABLE IV. Intra- and intermolecular vibrational frequencies and relative intensities for ground-state carbazole·Xe, in the frequency range 600–900 cm^{-1}. Intermolecular frequencies are derived from combination bands with intramolecular modes.

Assignment	Wave number/cm^{-1}	Interm./cm^{-1}	Intensity %[a]
ν_{14}	632.1		96.9
$\nu_3+\nu_7$	638.6		12.4
$3\cdot\nu_3$	643.1		31.8
ν_{15}	652.4		100.0
$\nu_{14}+\nu_y$	656.1	24.0	40.7
$3\cdot\nu_3+\nu_y$	667.7	24.7	11.1
	669.1		16.5
$\nu_{14}+\nu_z$	669.9	37.8	17.0
$\nu_{15}+\nu_y$	677.0	24.6	55.5
$\nu_{14}+2\cdot\nu_y^b$	681.2	49.1	33.2
$\nu_2+\nu_3+\nu_6$	683.4		11.5
$\nu_{15}+\nu_z$	689.9	37.5	20.9
$\nu_{14}+\nu_y+\nu_z^b$	692.5	60.4	14.2
$\nu_{15}+2\cdot\nu_y^b$	701.5	49.1	22.0
$\nu_{14}+3\cdot\nu_y^b$	705.4	73.3	13.4
$\nu_2+\nu_3+\nu_6+\nu_y$	707.7	24.3	13.4
$\nu_{15}+\nu_y+\nu_z^b$	712.7	60.3	11.8
$\nu_{14}+2\cdot\nu_y+\nu_z^b$	715.5	83.4	5.0
ν_{16}	745.0		15.0
	763.5		10.9
$\nu_3+\nu_{11}$	767.2		18.9
$\nu_{16}+\nu_y$	769.4	24.4	8.9
$\nu_3+\nu_{11}+\nu_y$	791.3	24.1	7.5
	830.1		5.5
	833.5		8.8
	836.2		7.0
$\nu_3+\nu_{14}$	845.2		56.1
ν_{21}	849.1		31.5
$\nu_5+\nu_{12}$	864.5		38.6
$\nu_3+\nu_{15}$	868.0		49.4
$\nu_3+\nu_{14}+\nu_y$	869.4	24.2	26.4
$\nu_{21}+\nu_y$	873.3	24.2	13.6
ν_{22}	881.6		43.1
$\nu_8+\nu_9$	885.0		11.9
$\nu_5+\nu_{12}+\nu_y$	889.2	24.7	11.5

[a]Percentage intensity, relative to strongest band.
[b]Tentative assignment.

C. Carbazole·Ar

1. S_0 ground-state vibrations

A brief discussion of intramolecular and vdW vibrations of Car·Ar, as shown in Fig. 3, was given in Ref. 21. The same intramolecular modes as for Car·Kr are observed for Car·Ar with similar relative intensities. The two strong bands at 214.8 cm^{-1} and 210.7 cm^{-1} correspond to intramolecular vibrations ν_3 and $2\cdot\nu_1$. Further bands in the spectrum below the dissociation limit are observed at 392.1 cm^{-1}, 427.1 cm^{-1}, and 430.5 cm^{-1} corresponding to intramolecular vibrations $\nu_2+\nu_4$, ν_7, and $2\cdot\nu_3$. Combination bands with intermolecular vibrations are considerably less intense for

Car·Ar than for Car·Kr and Car·Xe, reflecting smaller FC factors in the former case. The strongest vdW band is the $214.8+\nu_y$ transition, corresponding to a frequency of 22.9 cm^{-1} for the short-axis ν_y mode. A weaker level occurs closely above this transition, and is tentatively interpreted as a Fermi resonance of the ν_y fundamental with the fifth overtone of the long-axis in-plane mode, e.g., $214.8+6\cdot\nu_x$. The $214.8+\nu_z$ combination is also strong, yielding a frequency of 50.0 cm^{-1} for the out-of-plane ν_z fundamental. A weak band at 257.1 cm^{-1} is tentatively assigned as the $214.8+2\cdot\nu_y$ transition. The experimentally observed intermolecular frequencies in the S_0 and S_1 electronic states are collected in Table II.

TABLE V. Fluorescence lifetimes of carbazole and carbazole/rare gas complexes measured at the respective 0_0^0 bands.

Species	Lifetime (ns)	
carbazole	38 ± 2[a]	38 ± 2[b]
carbazole·Ne	35 ± 2[a]	
carbazole·Ar	26 ± 2[a]	26 ± 2[b]
carbazole·Kr	8 ± 1[a]	
carbazole·Xe	≈6[a]	

[a]This work.
[b]Reference 40.

2. Binding energies

The original bracketing measurements for this complex were previously presented in Ref. 21 and the corresponding dump spectrum is shown in Fig. 3. In contrast to Car·Kr and Car·Xe, vibrations above the dissociation limit are observed as *negative* signals in all dump spectra of this complex. This observation is rationalized as follows: The fluorescence quantum yield of Car·Ar is $\Phi_{fl}\approx0.61$ (see below). If the dump laser is not present or not resonant with any vibronic transition, the S_1 state population fluoresces to a large collection of levels according to the FC factors. That part of the population which fluoresces to ground-state levels below $D_0(S_0)$ creates a ''hot'' complex population, resulting in a constant background signal in the dump spectra. If the dump laser is resonant, a much larger fraction of the excited-state population will be dumped to one specific S_0 state vibrational level, since the stimulated emission rate is much higher than spontaneous emission, given the laser intensities used in our experiments. Hence, in the dump spectrum the background signal from hot complexes produced by fluorescence is decreased. This is overcompensated by an increase of signal from the population transferred to S_0, if this level is below D_0. The overall effect is an increase of signal and therefore a positive band is observed in the spectrum. If the dumped vibrational level is *above* D_0, where the excited population dissociates, the decrease of hot population generated by spontaneous emission processes is not compensated, resulting in an overall decrease of signal and a *negative* band in the spectrum. Negative bands in the dump spectra will only arise if the fluorescence quantum yield is high enough to generate a substantial background signal. As can be seen from Fig. 3, negative signals were observed for complexes with Ne and Ar, while for Kr and Xe no negative bands could be observed.

This explanation is in agreement with the measured fluorescence lifetimes of Car·R (R=Ne, Ar, Kr, Xe) complexes given in Table V. The measured S_1 lifetimes decrease in the series from Ne to Xe. Based on fluorescence lifetimes and quantum yield measurements of carbazole in hexane solution by Bolman,[45] we estimate a fluorescence quantum yield $\Phi_{fl}=0.9$ for gas phase carbazole. From the measured S_1 lifetimes we calculate fluorescence quantum yields of 0.83, 0.61, 0.19, and <0.14 for the Car·R (R=Ne, Ar, Kr, and Xe) complexes, respectively. Thus, the quantum yield Φ_{fl} of the Kr and Xe complexes is more than three times smaller than for the lighter adatoms, implying that other processes must compete with fluorescence emission. It seems reasonable that the ISC rate strongly increases when going from the Ne to the Xe complex, since spin–orbit coupling increases with Z^4.

Figure 3 shows that $D_0(S_0)$ falls into a spectral region which is relatively devoid of vibronic transitions, therefore the accuracy of the bracketing measurement is much lower than for the two heavier rare gases. From the spectrum in Fig. 3 the binding energy of Car·Ar was determined as $D_0(S_0)=517\pm37$ cm^{-1} in Ref. 21. In subsequent work, we were able to detect vibrationally hot carbazole released as a product from the VP process.[22] Analysis of that data yielded additional limits for the binding energy, and combination with the data of Ref. 21 allowed a much more accurate determination. The values determined[22] are $D_0(S_0)=530.4\pm1.5$ cm^{-1} for the S_0 state. Together with the measured spectral shift,[44] yields $D_0(S_1)=576.3\pm1.6$ cm^{-1} for the excited state (see Table III).

For the related vdW complex indole·Ar, Outhouse *et al.* have determined an upper limits for the S_0 and S_1 binding energies as $D_0(S_0)<502$ cm^{-1} and $D_0(S_1)<528$ cm^{-1}.[15] This is in qualitative agreement with the present results, since the carbazole molecule is larger by one benzene ring, offering an additional stabilization interaction in both states.

D. Carbazole·Ne

For this complex, the SEP-R2PI method furnished only an upper limit to the binding energy; in the dump spectra, no positive signals could be observed, while a *negative* signal was observed already at the 214.5 cm^{-1} band, as is shown in Fig. 3. The probe frequency was fixed 42 cm^{-1} to the red of the origin transition. We conclude that the Car·Ne dissociation energy is $D_0(S_0)<214.5\pm0.5$ cm^{-1}. By adding the spectral shift, $D_0(S_1)<222.9\pm1.0$ in the excited state S_1 (see Table III).

This clearly demonstrates one of the constraints of the experiment. The dissociation limit can only be bracketed if the complex has active modes above and below D_0. Also, the determination is more accurate for systems with a high density of active modes around D_0, as for Car·Kr and Car·Xe.

The upper limit to $D_0(S_1)$ given for Car·Ne in this work is in qualitative agreement with the excited-state dissociation energy of Ne bound to 2,3-dimethylnaphthalene (an aromatic molecule of comparable size to carbazole), which was deter-

mined from a three-dimensional quantum mechanical fit to the vdW vibrational level structure as $D_0(S_1)=179.2$ cm^{-1}.[46]

E. Correlation of results

1. Binding energies

Table III compiles the experimentally determined ground- and excited-state vdW binding energies for Car·R (R=Ne, Ar, Kr, and Xe). With the exception of Car·Ne, for which only upper limits were obtained, the binding energy measurements are very accurate. The relative errors for R=Ar and Xe are of the order of ±0.3%, and for R=Kr, of the order of ±0.7%.

The main contribution to the attractive intermolecular interaction of an aromatic molecule with a rare-gas atom are the dispersive interactions. The largest term is the induced dipole-induced dipole, which falls off with R^{-6}, followed by the induced dipole-induced quadrupole contribution, which falls of as R^{-8}. Due to the large dipole moment of carbazole (1.9 D, Ref. 36), the *dipole-induced dipole* interaction, proportional to R^{-6}, is also non-negligible. All of these interactions scale with the rare-gas atomic polarizability α_R, albeit with different dependencies on the distance of the atom from the carbazole center-of-mass R_{cm}. The distance dependencies are *not* simple R^{-n} functions, due to several factors; (i) the large size of the aromatic molecule, relative to R_{cm}, (the dipole–dipole dispersion term between two interacting atoms falls off with R^{-6}, while for an atom interacting with an infinite surface monolayer, the same *atomic* interaction term leads to an integrated interaction which is proportional to R^{-4}); the dispersive interaction of carbazole with a rare gas is an intermediate case; (ii) the distribution of polarizability and charge over the molecular frame, which is not homogeneous; (iii) the summation of attractive terms mentioned above.

Figure 7(a) shows the values of $D_0(S_0)$ and $D_0(S_1)$ plotted vs α_R (the polarizabilities are from Ref. 47). As expected, D_0 increases with the polarizability of R, going from Ar to Xe, but the increase is not linear. The deviation from linear behavior is significant for large values of α_R, e.g., R=Xe. This is an indication that the distance of the rare gas atom Ar, Kr or Xe, respectively, to carbazole, is different and increasing in the above order.

For Car·Ne the SEP-R2PI technique yields only upper limits to the vdW dissociation energy of the complex in the ground and first excited state (cf. Table III and Sec. III D). As expressed by the dashed straight lines in Fig. 7(a) (the upper line is for S_1, the lower for S_0 state, respectively), approximate lower limits can be derived for the Ne case, assuming linear dependence between D_0 and α_R for R=Ar. The values for Car·Ne obtained by this procedure are $D_0(S_0)>127$ cm^{-1} and $D_0(S_1)>139$ cm^{-1}, respectively.

Figure 7(b) plots the same D_0 values vs α_R/R_{cm}^6. For the R_{cm}, we have chosen to use the values of benzene·R determined by Neusser *et al.* by high resolution electronic spectroscopy[48] and by Brupbacher *et al.* by microwave spectroscopy,[20,49] since this is the most complete set of structural data currently available for an atom-large molecule complex. As outlined above, the choice of exponent is arbitrary, since there will be attractive contributions with exponents ranging from $n=4$ upwards. Despite these uncertainties, the plot of $D_0(S_0)$ vs α_R/R_{cm}^6 for carbazole·R (R=Ne, Ar, Kr, and Xe) results in an almost perfectly linearity cor-

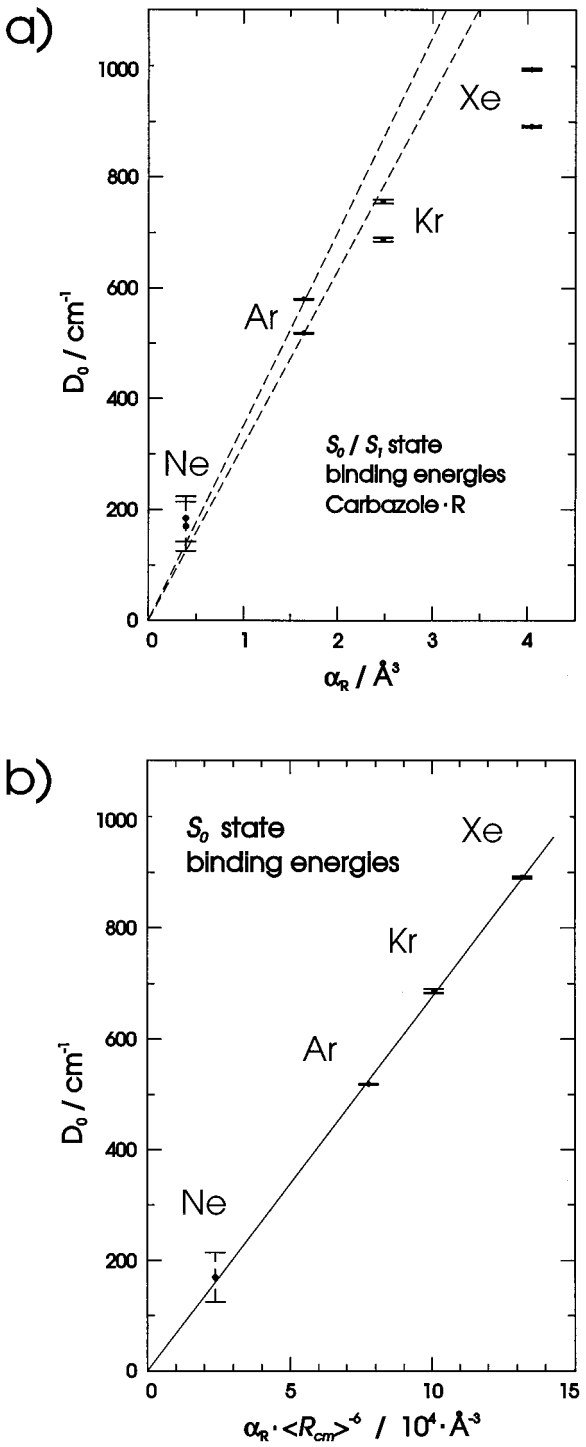

FIG. 7. (a) Experimental dissociation energies D_0 of carbazole·R (R=Ne, Ar, Kr, and Xe) vs polarizability (α_R) of the rare gas R in the ground (S_0) and first excited state (S_1), respectively. (b) Dissociation energies $D_0(S_0)$ (in cm^{-1}) vs α_R/R_{cm}^6. R_{cm} gives the distance of R to the carbazole center-of-mass. The error bars give the experimental uncertainties; the numerical values of D_0 are shown in Table III. For details, see text.

relation, cf. Fig. 7(b). Upon electronic excitation to the S_1 excited state, all D_0 values increase (Table III). The absolute increase in dissociation energy is experimentally determined by the spectral shifts $\delta\nu$. Such measurements have been performed for many vdW systems, and it has been known for over a decade that the shifts increase with polarizability.[50] It is interesting that also the *relative* increase is larger for the heavier atoms, increasing from 8.8% for Ar to 11.8% for Xe.

For carbazole-Ar a $R_{cm}(S_0)=3.48$ Å has recently been determined by Sussmann *et al.*;[51] the corresponding value for the complex with benzene is 3.58 Å.[48] The shorter vdW bond distance reflects the increased interaction strength with carbazole. This difference has not been accounted for in the plot of Fig. 7(b), since only the value for R=Ar is known.

Up to now, accurate experimental data available on dissociation energies of aromatic molecule-rare gas vdW complexes are not plentiful, and in many cases the accuracy of the data is not precisely known. Some early references are collected in Ref. 52. For the system Car·Kr, Bösiger and Leutwyler[36] previously determined $D_0(S_1)$ and $D_0(S_0)$; in the R2PI spectrum the signal strongly decreased between two bands at 736 cm^{-1} and 792 cm^{-1}, and moreover the band at 792 cm^{-1} was severely broadened. It was concluded that $D_0(S_1)$ is bracketed by these two values, resulting in binding energies of $D_0(S_1)=764\pm28$ cm^{-1} and $D_0(S_0)=696\pm28$ cm^{-1}. This is in good agreement with the value in this work [$D_0(S_0)=687.6\pm3.7$ cm^{-1}, see Table III].

As for the geometry determinations, many investigations of dissociation energies, some conflicting, have been undertaken for M=benzene. Brupbacher *et al.*[20] have deduced the binding energy of benzene·Ar and benzene·Ne by Fourier transform microwave spectroscopy and predict values of $D_0(S_0)=408$ cm^{-1} (R=Ar) and $D_0(S_0)=151$ cm^{-1} (R=Ne), respectively. Neusser *et al.*[48] predicted a much lower dissociation energy on the basis of an extrapolation of the out-of-plane vibrational mode. On the other hand, using pulsed field threshold ionization spectroscopy, the same group[37] has determined upper bounds for the ground state D_0: D_0(benzene·Ar)<457 cm^{-1} and D_0 (benzene·Kr)<402 cm^{-1}. Since D_0(benzene·Ar) must be smaller than D_0(benzene·Kr) they corrected the upper limit for the binding energy of benzene·Ar to D_0(benzene·Ar)<402 cm^{-1}. This value is in qualitative agreement with the work of Brupbacher and co-workers.[20] Given the fact that carbazole is larger than benzene, both values obtained for benzene·Ar are consistent with the present value for Car·Ar [$D_0(S_0)=530.4\pm1.5$ cm^{-1}, see Table III]. The upper bound for benzene·Kr, which is $D_0(S_0)<402$ cm^{-1} (Ref. 37) is much less than our value for Car·Kr of $D_0(S_0)=687.6$ cm^{-1}. Assuming that both values are correct, Kr is bound more than 1.7 times stronger to carbazole than to benzene.

On the theoretical side, *ab initio* calculations were performed on most benzene·R complexes. In a series of papers, Hobza and co-workers have presented ground-state well depths for benzene·Ne $D_e(S_0)=99$ cm^{-1}, benzene·Ar $D_e(S_0)=429$ cm^{-1} [$D_0(S_0)\approx380$ cm^{-1}], benzene·Kr $D_e(S_0)=485$ cm^{-1} [$D_0(S_0)\approx450$ cm^{-1}] and benzene·Xe $D_e(S_0)=601$ cm^{-1}.[16–18] These results were obtained using counterpoise corrected MP2 calculations. Klopper[19] and co-workers applied MP2-R12 (counterpoise corrected) to benzene·Ne and benzene·Ar and obtained ground-state value for D_e; $D_e(S_0)=154$ cm^{-1} (R=Ne) and $D_e(S_0)=553$ cm^{-1} (R=Ar). There is thus quite a large uncertainty in the *ab initio* results for the strongly studied benzene rare gas complexes; therefore, accurate experimental values are of high interest.

TABLE VI. Zero-point vibrational energies (ZPVE) and well depths D_e for carbazole·R (R=Ar, Kr, and Xe) in the S_0 and S_1 state.

Property	Ar	Kr	Xe
ZPVE(S_0)	38.5±2	33.6±2	33.6±2
$D_e(S_0)$	568.9±3.5	720.5±6.0	923.4±3.8
ZPVE(S_1)	39.4±2	34.9±2	35.2±2
$D_e(S_1)$	615.7±3.6	790.3±6.5	1030.0±4.6

2. Well depths

In order to determine the well depths D_e, accurate zero-point vibrational energies (ZPVE) are needed. In principle, these are only obtainable through knowledge of the exact intermolecular potential, in combination with a three-dimensionally exact vibrational eigenvalue calculation.[53] In the harmonic approximation, the observed ν_y and ν_z fundamentals yield the zero-point energy contributions. The zero-point energy for the ν_x vibration is very small, preliminary calculations give frequencies in the range 3–5 cm^{-1}.[53] We have therefore assumed $\nu_x/2=2.5$ cm^{-1} for the Car·Kr and Car·Xe complexes while for Car·Ar, $\nu_x/2$ was calculated from the observed (and tentatively assigned, cf. Table II) $6\cdot\nu_x$ frequency, assuming harmonic behavior. Frequency shifts of intramolecular vibrations upon complexation are neglected, since most frequencies of intramolecular modes are expected to shift very little when forming vdW complexes. The obtained zero-point vibrational energies (ZPVE) and well depths D_e are compiled in Table VI for the Car·Ar, Car·Kr, and Car·Xe complexes for both the S_0 and S_1 states. Interestingly, the ZPVE is largest for the Car·Ar complex and decreases by ≈10% for Car·Kr and Car·Xe. On going to the S_1 electronic state, the ZPVE increases only slightly (1–2 cm^{-1}). The relative difference between D_0 and $D_e[(D_e-D_0)/D_e]$ is 6.8% (6.4%), 4.6% (4.4%), and 3.6% (3.4%) for Car·Ar, Car·Kr, and Car·Xe in the $S_0(S_1)$ electronic state.

IV. CONCLUSIONS

The experimental results given in the above work show that the SEP-R2PI method is a flexible and accurate technique for the determination of the ground-state vdW dissociation energies $D_0(S_0)$ of M·R complexes. Very accurate determinations of the $D_0(S_0)$ values are presented for the systems carbazole·R (R=Ar, Kr, and Xe), with relative uncertainties of ±0.4%. For the complex with Ne an upper limit of $D_0(S_0)<214.5\pm0.5$ cm^{-1} is determined. By taking into account the S_0/S_1 electronic spectral shifts $\delta\nu$ of the complexes relative to bare carbazole, excited-state dissociation energies $D_0(S_1)$ were derived with similar precision.

The absolute accuracy of the dissociation energy determination depends on the density of optically active vibronic bands in the spectrum at the dissociation threshold. Furthermore, the dump spectra acquired with the SEP-R2PI technique yield mass-specific ground-state vibronic spectra of the M·R complexes.

No dependence of the dump spectra on the delay time between SEP (pump/dump) preparation process and R2PI probe step was observed on the time scale investigated, 50 ns$<\Delta<$15 μs. This is true for even the lowest excess energies studied, which for carbazole·Xe must be $<$3.2 cm^{-1}. We conclude that the vibrational predissociation lifetime is considerably less than 50 ns, even at these very low excess energies. Although this limit is not very stringent compared to the ps time scale studies in electronic excited states, it is not far above the *lower* VP lifetimes of 15 ns established by Weber and Rice for *s*-tetrazine/rare gas complexes.[8]

The measured dissociation energies $D_0(S_0)$ for Car·R (R=Ar, Kr, Xe) were found to depend linearly on $\alpha_R/R_{\rm cm}^6$, where α_R is the polarizability of R, and $R_{\rm cm}$ gives the distance of R from the center of mass of carbazole. This is in agreement with the assumption that the attractive vdW interaction between a rare gas atom and the carbazole molecule is dominated by the dipole–dipole dispersion term.

As potential advantages of the SEP-R2PI scheme we point out (i) SEP-R2PI is a mass-specific ground-state vibrational spectroscopic method at laser resolution. (ii) The method is optically triply resonant, and frequency specificity can be exploited in each of the three steps. (iii) Depending on the choice of the probe laser frequency, the method is essentially background-free and is therefore highly sensitive. Moreover, at the present signal levels the technique also allows to detect and analyze the aromatic molecule vibrational predissociation products, produced in the electronic ground-state, see Ref. 23.

Further applications of the SEP-R2PI technique to the measurement of dissociation energies D_0 of molecular van der Waals complexes and also of hydrogen-bonded complexes M·S (with S=H_2O, CH_3OH, and NH_3) are in progress.[53]

ACKNOWLEDGMENT

Support by the Schweiz. Nationalfonds (Project No. 20-33879-92) is gratefully acknowledged.

[1] M. Y. Hahn and R. L. Whetten, Phys. Rev. Lett. **61**, 1190 (1988).
[2] S. Leutwyler and J. Bösiger, Chem. Rev. **90**, 489 (1990).
[3] M. Schmidt, M. Mons, and J. LeCalvé, Chem. Phys. Lett. **177**, 371 (1991).
[4] J. E. Kenny, D. V. Brumbaugh, and D. H. Levy, J. Chem. Phys. **71**, 4757 (1979); J. A. Blazy and D. H. Levy, *ibid*. **76**, 4328 (1982); D. V. Brumbaugh, J. E. Kenny, and D. H. Levy, *ibid*. **78**, 3415 (1983).
[5] E. R. Bernstein, K. Law, and M. Schauer, J. Chem. Phys. **80**, 107 (1984); M. Schauer, K. Law, and E. R. Bernstein, *ibid*. **81**, 49 (1984); **82**, 726 (1985).
[6] D. F. Kelley and E. R. Bernstein, J. Phys. Chem. **90**, 5164 (1986).
[7] K. W. Butz, D. L. Catlett, Jr., D. E. Ewing, D. Krajnovich, and C. S. Parmenter, J. Phys. Chem. **90**, 3533 (1986); H.K. O, C. S. Parmenter and M. C. Su, Ber. Bunsenges. Phys. Chem. **92**, 253 (1988).
[8] P. M. Weber and S. A. Rice, J. Chem. Phys. **88**, 6107, 6121 (1988); **88**, 6120 (1988).
[9] S. H. Kable, J. W. Thoman, and A. E. W. Knight, J. Chem. Phys. **88**, 4748 (1988).
[10] D. O. DeHaan and T. S. Zwier, J. Chem. Phys. **90**, 1460 (1989).
[11] M. R. Nimlos, M. A. Young, E. R. Bernstein, and D. F. Kelley, J. Chem. Phys. **91**, 5268 (1989).
[12] J. C. Alfano, S. J. Martinez III, and D. H. Levy, J. Chem. Phys. **91**, 702 (1989); **94**, 1673 (1990).
[13] S. A. Wittmeyer, A. J. Kaziska, A. M. Motyka, and M. R. Topp, Chem. Phys. Lett. **154**, 1 (1989).
[14] D. H. Semmes, J. S. Baskin, and A. H. Zewail, J. Am. Chem. Soc. **109**, 4104 (1987); D. H. Semmes, J. S. Baskin, and A. H. Zewail, J. Chem. Phys. **92**, 3359 (1990).
[15] E. A. Outhouse, G. A. Bickel, D. R. Demmer, and S. C. Wallace, J. Chem. Phys. **95**, 6261 (1991).
[16] P. Hobza, H. L. Selzle, and E. W. Schlag, J. Chem. Phys. **95**, 391 (1991).
[17] P. Hobza, O. Bludsky, H. L. Selzle, and E. W. Schlag, J. Chem. Phys. **97**, 335 (1992).
[18] O. Bludsky, V. Spirko, V. Hrouda, and P. Hobza, Chem. Phys. Lett. **196**, 410 (1992).
[19] W. Klopper, H. P. Lüthi, Th. Brupbacher, and A. Bauder, J. Chem. Phys. **101**, 9747 (1994).
[20] Th. Brupbacher, J. Makarewicz, and A. Bauder, J. Chem. Phys. **101**, 9736 (1994).
[21] T. Bürgi, T. Droz, and S. Leutwyler, Chem. Phys. Lett. **225**, 352 (1994).
[22] T. Droz, T. Bürgi, and S. Leutwyler, Ber. Bunsenges. Phys. Chem. **99**, 429 (1995).
[23] T. Bürgi, T. Droz, and S. Leutwyler (in preparation).
[24] C. E. Hamilton, J. L. Kinsey, and R. W. Field, Annu. Rev. Phys. Chem. **37**, 493 (1986).
[25] T. Ebata, M. Furukawa, and M. Ito, J. Opt. Soc. Am. B **7**, 1890 (1990).
[26] M. Takayanagi and I. Hanazaki, J. Opt. Soc. Am. B **7**, 1898 (1990).
[27] F. J. Northrup and T. J. Sears, Annu. Rev. Phys. Chem. **43**, 125 (1992).
[28] D. Frye, P. Arias, and H.-L. Dai, J. Chem. Phys. **88**, 7240 (1988); D. Frye, L. Lappierre, and H.-L. Dai, J. Opt. Soc. Am. B **7**, 1905 (1990).
[29] M. Berry, R. A. Loomis, L. C. Giancarlo, and M. I. Lester, Chem. Phys. Lett. **178**, 301 (1991); M. Berry, M. R. Brustein, M. I. Lester, C. Chakravarty, and D. C. Clary, J. Chem. Phys. **96**, 7890 (1992).
[30] (a) L. L. Connell, S. M. Ohline, P. W. Joireman, T. C. Corcoran, and P. M. Felker, J. Chem. Phys. **96**, 2585 (1992); (b) P. M. Felker, J. Phys. Chem. **96**, 7844 (1992); (c) S. M. Ohline, J. Romascan, and P. M. Felker, Chem. Phys. Lett. **207**, 563 (1993).
[31] V. A. Venturo, P. M. Maxton, and P. M. Felker, J. Phys. Chem. **96**, 5234 (1992); Chem. Phys. Lett. **198**, 628 (1992).
[32] V. A. Venturo and P. M. Felker, J. Phys. Chem. **97**, 4882 (1993).
[33] M. F. Hineman, E. R. Bernstein, and D. F. Kelley, J. Chem. Phys. **101**, 850 (1994).
[34] P. G. Smith and M. R. Topp, Chem. Phys. Lett. **229**, 21 (1994).
[35] M. Takayanagi and I. Hanazaki, Chem. Phys. Lett. **190**, 115 (1992); J. Chem. Phys. **98**, 6958 (1993).
[36] J. Bösiger and S. Leutwyler, Chem. Phys. Lett. **126**, 238 (1986).
[37] H. Krause and H. J. Neusser, J. Chem. Phys. **97**, 5923 (1992); **99**, 6278 (1993).
[38] M. Mandziuk and Z. Bacic, J. Chem. Phys. **98**, 7165 (1993).
[39] M. Mandziuk, Z. Bacic, T. Droz, and S. Leutwyler, J. Chem. Phys. **100**, 52 (1994).
[40] R. Knochenmuss and S. Leutwyler, J. Chem. Phys. **92**, 4689 (1990).
[41] A. Bree and R. Zwarich, J. Chem. Phys. **51**, 903 (1969).
[42] E. Honegger, R. Bombach, and S. Leutwyler, J. Chem. Phys. **85**, 1234 (1986).
[43] T. Bürgi and S. Leutwyler (unpublished).
[44] J. Bösiger and S. Leutwyler, Z. Phys. Chem. NF **154**, 31 (1987).
[45] I. B. Bolman, J. Phys. Chem. **74**, 3085 (1970).
[46] T. Droz, S. Leutwyler, M. Mandziuk, and Z. Bacic, J. Chem. Phys. (in press).
[47] G. M. Barrow, in *Physical Chemistry* (McGraw–Hill, Koyakusha, 1973).
[48] H. J. Neusser, R. Sussmann, A. M. Smith, E. Riedle, and Th. Weber, Ber. Bunsenges. Phys. Chem. **96**, 1252 (1992).
[49] T. Brupbacher and A. Bauder, Chem. Phys. Lett. **173**, 435 (1990).
[50] A. T. Amos, Chem. Phys. Lett. **126**, 107 (1986).
[51] R. Sussmann and H. J. Neusser, Chem. Phys. Lett. **221**, 46 (1994).
[52] S. Leutwyler and J. Jortner, J. Phys. Chem. **91**, 5558 (1987).
[53] T. Bürgi, T. Droz, and S. Leutwyler (in preparation).